Available online at www.sciencedirect.com
ScienceDirect
Journal of Power Sources 176 (2008) 1–8
JOURNAL OF POWER SOURCES
www.elsevier.com/locate/jpowsour

Synthesis, electrical and electrochemical properties of $Ba_{0.5}Sr_{0.5}Zn_{0.2}Fe_{0.8}O_{3-\delta}$ perovskite oxide for IT-SOFC cathode

Bo Wei [a,*], Zhe Lü [a], Xiqiang Huang [a], Mingliang Liu [a], Na Li [a], Wenhui Su [a,b,c]

[a] *Center for Condensed Matter Science and Technology, Harbin Institute of Technology, Harbin 150001, PR China*
[b] *Department of Physics, Jilin University, Changchun 130023, PR China*
[c] *International Center for Materials Physics, Chinese Academy of Sciences, Shenyang 110015, PR China*

Received 2 July 2007; received in revised form 22 September 2007; accepted 24 September 2007
Available online 30 October 2007

Abstract

The $Ba_{0.5}Sr_{0.5}Zn_{0.2}Fe_{0.8}O_{3-\delta}$ (BSZF) complex oxide with cubic perovskite structure was synthesized and examined as a new cobalt-free cathode for intermediate-temperature solid oxide fuel cells (IT-SOFCs). The electrical conductivity was relatively low with a peak value of 9.4 S cm^{-1} at about 590 °C, which was mainly caused by the high concentration of oxygen vacancy and the doping of bivalent zinc in B-sites. At 650 °C and under open circuit condition, symmetrical BSZF cathode on Sm-doped ceria (SDC) electrolyte showed polarization resistances (R_p) of 0.48 Ω cm^2 and 0.35 Ω cm^2 in air and oxygen, respectively. The dependence of R_p with oxygen partial pressure indicated that the rate-limiting step for oxygen reduction was oxygen adsorption/desorption kinetics. Using BSZF as the cathode, the wet hydrogen fueled Ni + SDC anode-supported single cell exhibited peak power densities of 392 mW cm^{-2} and 626 mW cm^{-2} at 650 °C when stationary air and oxygen flux were used as oxidants, respectively.

Keywords: Solid oxide fuel cells; Cathode; $Ba_{0.5}Sr_{0.5}Zn_{0.2}Fe_{0.8}O_{3-\delta}$; Electrical conductivity; Electrochemical performance

1. Introduction

Intermediate-temperature solid oxide fuel cells (IT-SOFCs) operating at 500–800 °C have attracted considerable interest in recent years [1–3]. Lowering the operation temperature can minimize various problems associated with high temperature operation, such as the ionic interdiffusions between electrode/electrolyte interfaces, sintering of electrodes. In addition, advantages including the use of inexpensive stainless steel as the interconnect, lower operating cost and fast starting time are also driving forces for research of IT-SOFCs. Regarding the solid electrolyte, Sm-/Gd-doped ceria (SDC/GDC) or Sr-, Mg- co-doped lanthanum gallate (LSGM) electrolytes with significantly higher ion conductivity than yttria-stabilized zirconia (YSZ) are suitable for the lower temperature operation [4]. For cathode, traditional $La_xSr_{1-x}MnO_3$ (LSM) perovskites are widely regarded as one of the most promising cathodes with good performance at around 800 °C [5]. With the decrease of temperature, however, the cathode overpotential of LSMs increases dramatically mainly due to the relatively low values of oxygen surface exchange coefficient and the oxygen diffusion coefficient [6]. It is, therefore, of great importance to develop high performance cathode materials for the IT-SOFCs.

Perovskite-type mixed ionic and electronic conductors (MIECs) have been widely investigated as potential cathodes operated in the intermediate temperature range. Considerable interest is devoted to cobalt-containing perovskite-type oxides, such as $Sm_{0.5}Sr_{0.5}CoO_{3-\delta}$ (SSC) [7,8], $La_xSr_{1-x}Co_yFe_{1-y}O_{3-\delta}$ (LSCF) [9–11] and $Ba_{0.5}Sr_{0.5}Co_{0.8}Fe_{0.2}O_{3-\delta}$ (BSCF) [12–14], etc. Oxygen-deficient MIECs can simultaneously transport electron and oxygen ion defects, which greatly extends the active sites from traditional triple phase boundaries (TPBs) at the cathode/electrolyte interface to the entire surface of the porous cathode. The TPBs length of MIEC cathodes can be orders of magnitude higher than traditional LSM cathodes. Therefore, these MIEC cathodes can exhibit higher electro-catalysis properties toward oxygen reduction than LSMs cathodes. However, these cobalt-based cathodes often suffer some problems like high thermal expansion coefficients (TECs) and high cost of cobalt element. In recent years, many

* Corresponding author. Tel.: +86 451 8641 8420; fax: +86 451 8641 2828.
E-mail address: wavingwei@126.com (B. Wei).

0378-7753/$ – see front matter © 2007 Elsevier B.V. All rights reserved.
doi:10.1016/j.jpowsour.2007.09.120

cobalt-free perovskite-type materials were reported for the cathodes of IT-SOFC, such as $La_xSr_{1-x}FeO_{3-\delta}$ (LSF) [15,16], $La_xSr_{1-x}Fe_yNi_{1-y}O_{3-\delta}$ (LSNF) [17,18], $Pr_{0.7}Sr_{0.3}Fe_{1-x}Ni_xO_{3-\delta}$(PSFN) [19], $La_xSr_{1-x}CuO_{2.5-\delta}$ [20], etc. For example, the polarization resistance of the 40 wt% LSF-YSZ cathode was found to be approximately 0.1 Ω cm at 700 °C [21]. On SDC electrolyte, the polarization resistances of pure $La_{0.4}Sr_{0.6}Ni_{0.2}Fe_{0.8}O_{3-\delta}$ (LSNF) and LSNF-45 vol.% SDC composite cathodes were measured to be about 0.5 Ω cm and 0.16 Ω cm at 700 °C, respectively [18].

Recently, Wang et al. have developed the $Ba_{0.5}Sr_{0.5}Zn_{0.2}Fe_{0.8}O_{3-\delta}$ (BSZF) perovskite oxide as a novel cobalt-free oxygen permeable membrane, based on the fact that $SrFeO_{3-\delta}$ is a mixed conductor [22]. At 950 °C, BSZF membrane exhibited higher oxygen-permeation flux (1.45 mm in thickness, 0.35 ml min^{-1} cm^{-2}) than that of $La_{0.6}Sr_{0.4}Co_{0.2}Fe_{0.8}O_{3-\delta}$ (1 mm in thickness, 0.25 ml min^{-1} cm^{-2}). Furthermore, it showed good chemical stability even under low oxygen partial pressure of 10^{-12} atm, which is also preferred for SOFC cathodes. Considering that LSCF is widely used for IT-SOFC cathode, herein we tried to investigate BSZF as a novel cobalt-free cathode IT-SOFCs. The BSZF powder was synthesized via wet chemical method and its electrical conductivity and electrochemical performance were characterized in detail to investigate its suitability as the cathode of IT-SOFCs.

2. Experimental

2.1. Preparation of the BSZF powder

The powder of $Ba_{0.5}Sr_{0.5}Zn_{0.2}Fe_{0.8}O_{3-\delta}$ was synthesized by the modified sol–gel method using combined citric acid and ethylenediamine tetraacetic acid (EDTA) complexing agents. A flowchart is given in Fig. 1 for the preparation of the BSZF powder. The starting materials were $Ba(NO_3)_2$, $Sr(NO_3)_2$, $Zn(NO_3)_2{\cdot}6H_2O$, $Fe(NO_3)_3{\cdot}9H_2O$, EDTA, citric acid and ammonia, all of which were analytical reagent grade (>99%). The desired amounts of metal nitrates were first dissolved in EDTA-$NH_3{\cdot}H_2O$ solution (heated at 80 °C). Then, a certain amount of citric acid was added with a molar ratio of EDTA:citric acid:total metal ions of 1:1.5:1. After the evaporation of water, a viscous brown gel was obtained, which was subsequently kept at 150 °C overnight and resulted in a sponge-like dry precursor. After heat-treatment at 950 °C for 5 h in a muffle furnace, black BSZF powder was obtained and its crystal structure was examined by a Shimadzu XRD-6000 X-ray powder diffractometer (XRD, Cu Kα radiation, λ = 0.15418 nm). Thermogravimetry analysis (TGA) of calcined BSZF powder was performed by a TA SDT2960 from room temperature to 1000 °C in air (heating rate = 10 °C min^{-1}, flow rate = 100 ml min^{-1}).

2.2. Electrical conductivity measurement

The phase-pure BSZF powder was pressed uniaxially at 300 MPa and sintered at 1170 °C for 10 h with a heating/cooling rate of 2 °C min^{-1}. The relative density of BSZF pellet was about 96.5%, as measured by the standard Archimedes method using purified water. Electrical conductivity was measured using the four-probe method from room temperature to 900 °C in air, using a Keithley 2400 sourcemeter and a Yuguang AI 808P programmed-temperature controller.

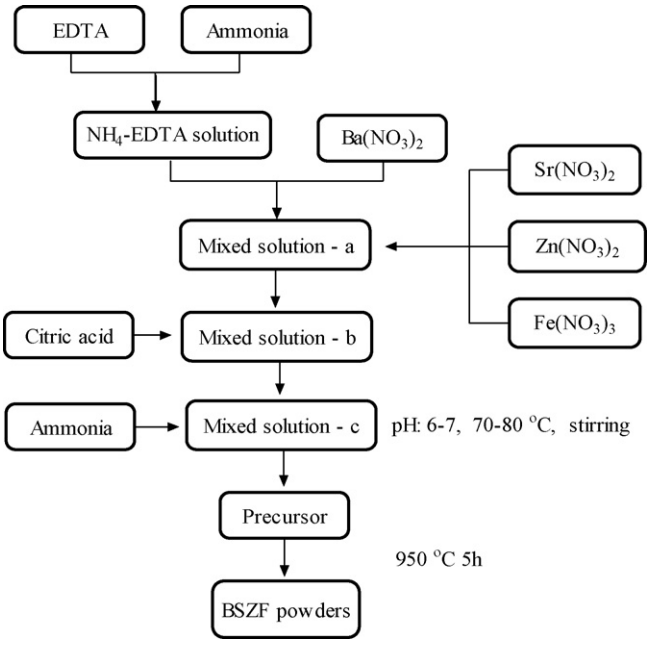

Fig. 1. Procedure for preparation of the BSZF powder.

2.3. Electrochemical and microstructure characterizations

The $Sm_{0.2}Ce_{0.8}O_{1.9}$ (SDC) powder, prepared from citrate-combustion method, was pressed into pellets at 200 MPa and sintered at 1400 °C for 4 h, serving as the substrates for symmetric cell. The diameter and thickness of sintered SDC pellets were 10.2 mm and 0.5 mm, respectively, with a relative density of ~98%. The anode-supported SDC bilayer was prepared by a so-called dry-pressing method [23]. NiO + SDC mixture (65%: 35% in weight with certain pore former) was pre-pressed at 200 MPa as substrate. Then loose SDC powder, synthesized by glycine-nitrite process (GNP), was uniformly distributed onto anode substrate, co-pressed at 250 MPa and sintered subsequently at 1400 °C for 4 h to densitify the SDC film. The diameter and thickness of the sintered anode-supported cell were 10.5 mm and 0.6 mm, respectively. The cathode slurry was prepared by mixing the thoroughly ground BSZF powder with organic binder (6 wt% ethyl cellulose and terpineol). The slurry was painted on both side of the dense SDC disks or on the center of SDC film and dried subsequently at about 150 °C for half an hour. Finally, BSZF cathodes were calcinated at 950 °C for 4 h in stagnant air with heating and cooling rates of 2–3 °C min^{-1}. The cathode effective areas were about 0.16 cm^2.

For electrochemical characterizations, silver paste (DAD-87, Shanghai Research Institute of Synthetic Resins) was coated on the electrode surfaces as the current collector. The performances of BSZF half-cell and single cell were determined by the combined system with a Solartron SI 1260 impedance/gain-phase

analyzer and a Solartron SI 1287 electrochemical interface. Electrochemical impedance spectra (EIS) were obtained in the frequency range of 91 kHz to 0.1 Hz with ac signal amplitude of 10 mV under open-circuit conditions. The Z-view 2.3 software was used to analyze the obtained impedance spectra. For BSZF/SDC/BSZF cell testing, the cathode was evaluated in two-electrode symmetric cell configuration. Impedance spectra were obtained in oxygen–nitrogen mixtures controlled by a mass flow controller (D08-4D/2M, Seven Star Huachuang). An yttria-stabilized zirconia sensor was used to monitor the in situ oxygen partial pressure. For single cell testing, the anode side of the pellet was sealed on one end of the alumina tube using silver paste. The cell was measured by four-probe configuration. The anode compartment was fed by humidified hydrogen with 3 vol.% H_2O at the flow rate of 100 ml min^{-1}, while the cathode was exposed to stationary air or oxygen (100 ml min^{-1}) as oxidants. Microstructures of the BSZF powder, BSZF symmetric cell and single cell were observed by a Hitachi S-570 scanning electron microscope (SEM).

3. Results and discussion

3.1. Powder characterizations

Fig. 2 presents XRD pattern of the BSZF powder after calcination at 950 °C for 5 h. Sharp lines reflect a well-developed crystallization and all the peaks can be well indexed as a cubic perovskite structure with the space group of $Pm3m$(2 1 1), indicating that its Goldschmidt tolerance factor is around 1. The lattice parameter and the cell volume of BSZF are calculated to be $a = 0.398$ nm and $V = 0.063$ nm^3, respectively. Fig. 3 shows the SEM micrograph of the as-synthesized BSZF powder. A coral-like structure can be clearly observed with many pores at the micrometer scale that left by the burning of organics. The walls are very thin and the porous structure can be easily crushed to fine powder.

Fig. 4 shows the temperature dependences weight change and oxygen content for BSZF powder in air. It can be clearly identified that the weight loss continues with the increasing of temperature, which is primary associated with the loss of lattice oxygen and the formation of oxygen vacancy, as described in the Krönger–Vink notation:

$$2Fe_{Fe}^{\bullet\bullet}O_o^{\times} \overset{\text{heating}}{\longleftrightarrow} 2Fe_{Fe}^{\times} + V_o^{\bullet\bullet} + 1/2O_2(g) \quad (1)$$

The non-stoichiometry of BSZF at room temperature was determined to be as high as 0.412 [24], and the oxygen stoichiometry reaches the very low value of about 2.35 at 1000 °C. Note that although the oxygen vacancy concentration is very high at elevated temperature, BSZF perovskite still kept a cubic perovskite structure up to 1000 °C as confirmed by the in situ high-temperature XRD technique [22]. This means that the oxygen vacancies in BSZF lattices are disordered, and therefore, it can be assumed that the ion diffusion rate is high, which is favorable for the oxygen reduction reaction.

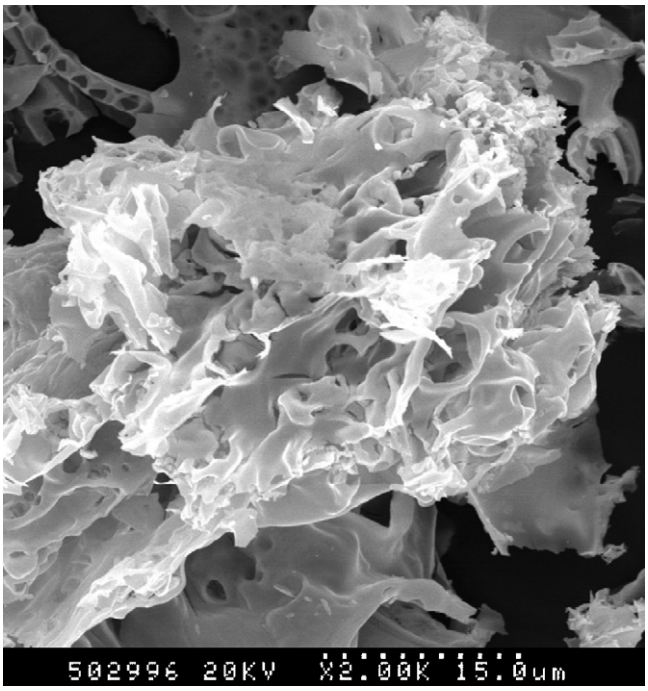

Fig. 3. SEM image of the as-prepared BSZF powder.

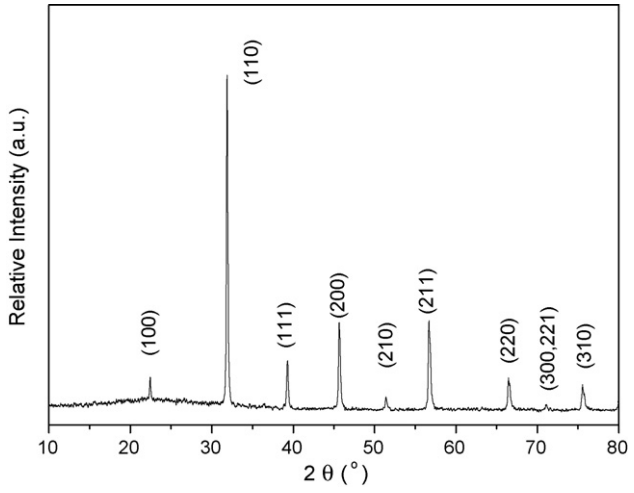

Fig. 2. X-ray diffraction pattern of BSZF powder.

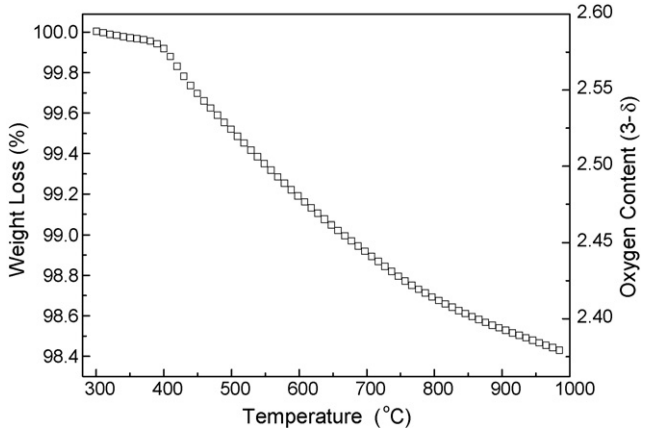

Fig. 4. Weight change and oxygen content of the BSZF powder as a function of temperature.

3.2. Electrical conductivity

For perovskite MIECs, the co-presence of electronic holes and oxygen vacancies makes them simultaneously exhibit both electronic and ionic conductivity. As electronic conductivity is at least one order higher than ionic conductivity, the measured values (total conductivity) can be mainly referred to electronic conductivity. Fig. 5 shows the temperature dependence of electrical conductivity of dense BSZF pellet in air. It can be found in Fig. 5a that, upon heating, the conductivity increases with the increasing of temperature (p-type semi-conductivity) and reaches the maximum value of 9.4 S cm^{-1} at about 590 °C, after which, the conductivity begins to decrease (pseudometallic behavior). The decrease of the conductivity is mainly associated with the loss of the lattice oxygen and the reduction of the B-site iron ions at elevated temperature.

The reasons for the relatively low conductivity of BSZF can be mainly intercepted as follows. The first one is the high vacancy concentration in BSZF lattice. As discussed above, there is large concentration of oxygen vacancy, which will lead to the significantly decrease in charge carriers concentration and the perturbation the O–(Fe, Zn)–O periodic potential [25]. In addition, the vacancies also can act as the scattering centers, or as random traps for electrons, resulting in the decrease of the carrier mobility [26]. The second reason can be ascribed to the fact that zinc holds fixed bivalent state, which will not contribute to conductivity. The conductivity of strontium ferrites ($SrFeO_{3-\delta}$) was reported as about 17.3 S cm^{-1} at 700 °C [27]. With zinc doping in B-sites, the conductivity will decrease as expected, due to the decrease of the total concentration of B-sites that participate in the electronic transport processes. Similar results were observed in Al doped $SrFeO_{3-\delta}$ system; the conductivity decreased with the increase of the Al content. The Mössbauer spectroscopy results indicated that the concentration of electron holes localized on iron cations [28] .It could be assumed that similar localization may be occurred in BSZF lattices.

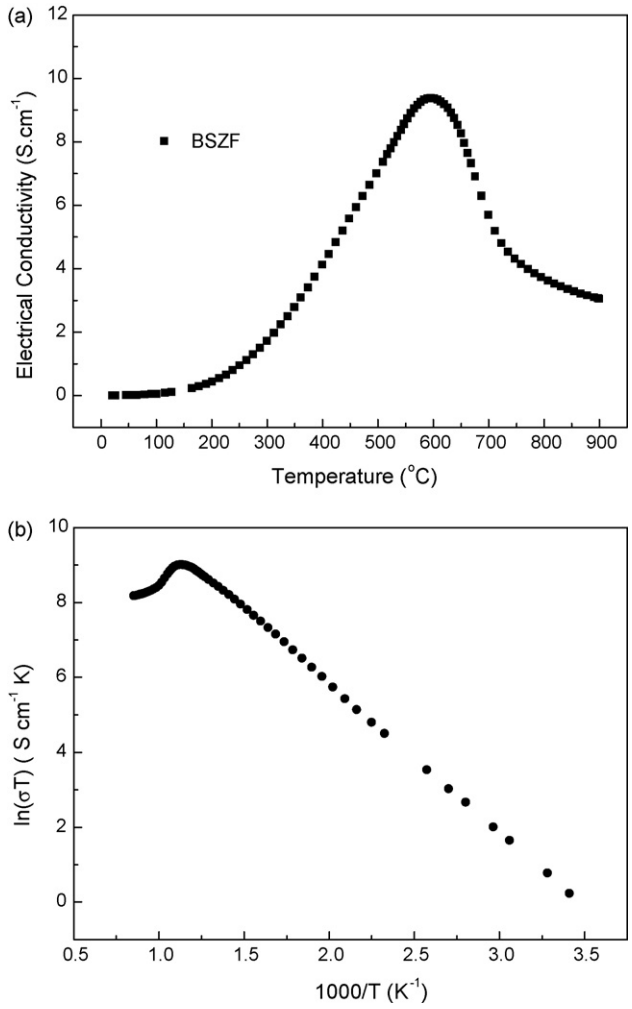

Fig. 5. Electrical conductivity of the BSZF perovskite pellet: (a) conductivity as a function of the temperature and (b) ln σT vs. 1000/T plot. The measurement was carried out in air.

The conductivity of BSZF is relative low, and several perovskite electrode materials with low conductivity have reported with good electrochemical performances. For example, the maximum conductivities of $Ba_xSr_{1-x}Co_{0.8}Fe_{0.2}O_{3-\delta}$ (BSCF) were about 20–60 S cm^{-1} [29]. The conductivity of $La_{0.75}Sr_{0.25}Cr_{0.5}Mn_{0.5}O_3$ (LSCM) anode under working condition ($P_{O_2} = 10^{-20}$ atm) was about 3 S cm^{-1} at 800 °C [30]. With well-coated current collector, the current is expected to pass across the porous electrode without distributing on the surface (minimizing the sheet resistance). Compared with the electronic conductivity (total conductivity), the ionic conduction related to large oxygen vacancy concentration should be more important for SOFC cathode. In the following section, we can found that BSZF cathode exhibits attractive electrochemical performances for oxygen reduction. For $Ba_{0.5}Sr_{0.5}Co_{0.8}Fe_{0.2}O_{3-\delta}$ cathode, we have found that the doping of trivalent rare earth element, like Sm^{3+}, will obviously increase the electrical conductivity while maintain high electrochemical performance [31,32]. So the conductivity of BSZF is excepted to be enhanced with certain rare earth element doping.

The Arrhenius plot of BSZF pellet is given in Fig. 5b. The linear part can be described by the small polaron conduction mechanism, following the formula: $\sigma = (A/T)\exp(-E_a/kT)$, where A is material constant including the carrier concentration term, E_a the activation energy, k the Boltzmann's constant and T is the absolute temperature. The activation energy calculated from the linear fit is 32.80 ± 0.02 kJ mol^{-1}.

3.3. Electrochemical impedance spectra of symmetric cell

In order to understand the mechanism of oxygen reduction at the BSZF cathode, impedance measurements were carried out as the function of oxygen partial pressure. Fig. 6 shows the typical impedance spectra of BSZF cathode obtained in various oxygen partial pressures at 650 °C. There are at least two highly overlapped arcs for these spectra, while it is difficult to distinguish the high- and low-frequency arc with reasonable accuracy. The polarization resistance increases from 0.34 Ω cm^2 at 0.95 atm (in oxygen) to 2.03 Ω cm^2 at 0.009 atm (in nitrogen). Especially, the low-frequency arc changes significantly with the decreasing of oxygen content, suggesting the gas diffusion related processes primarily dominate the cathode reaction. The equa-

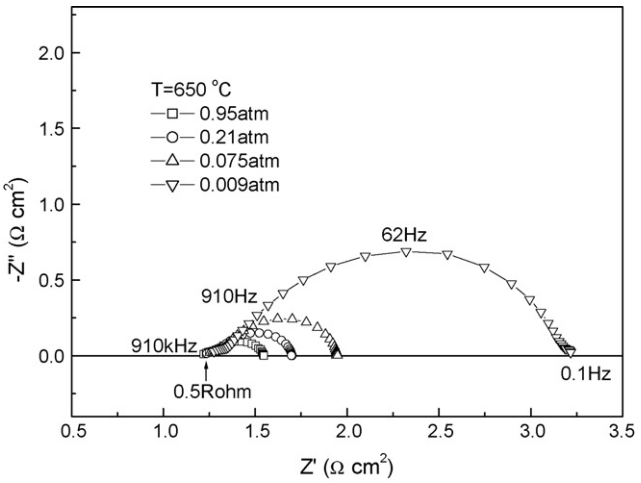

Fig. 6. Typical impedance spectra of the BSZF cathode obtained in various oxygen partial pressures ($T = 650\,^{\circ}C$).

tion, $R_p = R_p^0(P_O)^{-m}$, is widely used to describe the change of electrode resistance with oxygen partial pressure [33] .The magnitude of m provides useful insight into the rate-limiting step of oxygen reduction at cathode. Generally, $m = 0.25$ has been associated with the charge-transfer process at the TPBs, while $m = 0.5$ with oxygen adsorption/desorption processes, and $m = 1$ with gaseous diffusion of oxygen molecules in porous cathode. Fig. 7 shows the oxygen partial pressure dependence of cathodic R_p of BSZF cathode at various temperatures (550–800 °C). The m values vary between 0.53 and 0.40 in the measured temperature range, exhibiting a dependence close to $(P_{O_2})^{0.5}$. This indicates that, for BSZF cathode, the oxygen surface exchange process primarily dominates the oxygen reduction reactions. Our results are similar to other MIEC cathodes. Zhao et al. have observed a $(P_{O_2})^{0.5}$ dependence for $La_{0.6}Sr_{0.4}Co_{0.2}Fe_{0.8}O_3$–$Ce_{0.7}Bi_{0.3}O_2$ (LSCF–CBO) composite cathode [34]. Shao and Haile have confirmed that the oxygen diffusion in BSCF cathode was rapid and the surface exchange kinetics was rate determining, as measured by both impedance spectra and oxygen permeability [12].

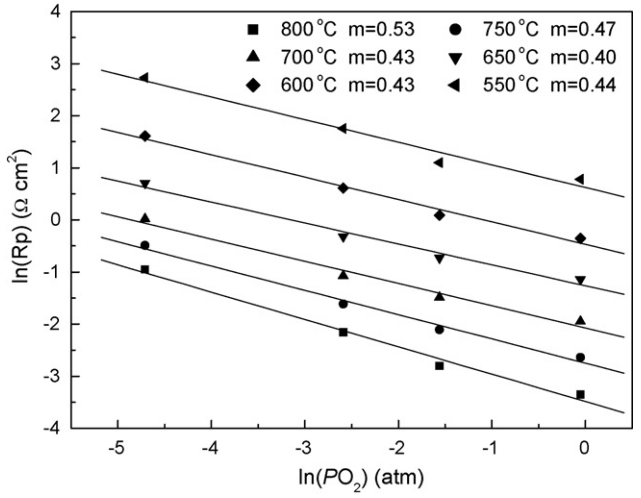

Fig. 7. Oxygen partial pressure dependence of cathodic R_p for BSZF cathode at various temperatures.

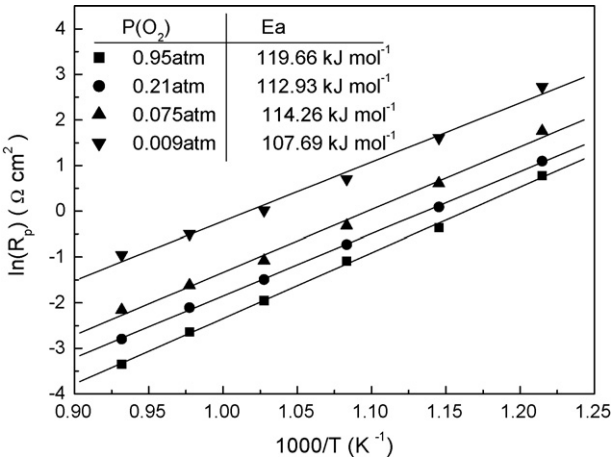

Fig. 8. Arrhenius plots of the BSZF cathode operated in various oxygen partial pressures.

The observed polarization resistances (R_p) for BSZF cathode are as low as $0.23\,\Omega\,cm^2$, $0.48\,\Omega\,cm^2$ and $1.06\,\Omega\,cm^2$ at 700 °C, 650 °C and 600 °C, respectively. These values are much lower than conventional $La_{0.7}Sr_{0.3}MnO_3$ (LSM) cathode measured under same conditions, which exhibits polarization resistances of $2.40\,\Omega\,cm^2$, $4.88\,\Omega\,cm^2$, $9.97\,\Omega\,cm^2$ at corresponding temperatures [24]. As both A-site cations of BSZF are alkaline-earth elements, similar to BSCF, there is a large concentration of oxygen vacancies in BSZF and the electrochemically active sites are extended to the whole porous cathode, which makes BSZF cathode exhibit higher performance than LSM cathodes. Comparing to the other cobalt-free cathodes, for example, the R_p of $La_{0.4}Sr_{0.6}Ni_{0.2}Fe_{0.8}O_{3-\delta}$ cathode on SDC were about $0.5\,\Omega\,cm^2$ at 700 °C and $0.1\,\Omega\,cm^2$ at 800 °C [18]. For common used cobalt-containing $La_{0.6}Sr_{0.4}Co_{0.2}Fe_{0.8}O_{3-\delta}$ − 30 wt%GDC cathode, the polarization resistances were about $0.6\,\Omega\,cm^2$ at 590 °C and less than $0.1\,\Omega\,cm^2$ at 690 °C [9]. Obviously, the activity of BSZF cathode is higher than traditional LSMs and other cobalt-free cathodes. The performance of BSZF is also comparable to cobalt-containing cathode.

Fig. 8 shows the Arrhenius plots of the BSZF cathode tested in various oxygen partial pressures. Good linear relation can be found, and single slope implies that the same reaction mechanism controls the overall electrode behavior in the temperature range and P_{O_2} studied. The activation energies (E_a) calculated from the slope of the curves change small with oxygen partial pressures. The specific values are $112.9 \pm 1.3\,kJ\,mol^{-1}$, $119.8 \pm 2.2\,kJ\,mol^{-1}$ for the BSZF cathode in air (0.21 atm) and oxygen (0.95 atm), respectively.

3.4. Microstructure

Fig. 9 illustrates the SEM micrographs of the BSZF cathode fired at 950 °C for 4h. Clearly, porous BSZF cathode exhibits good, continuous contact with dense SDC substrate. The microstructure appears to be homogeneous with well-necked grains (about 1–2 μm). Fig. 10 shows the cross-sectional view of the Ni + SDC anode-supported single cell. The adhesion of

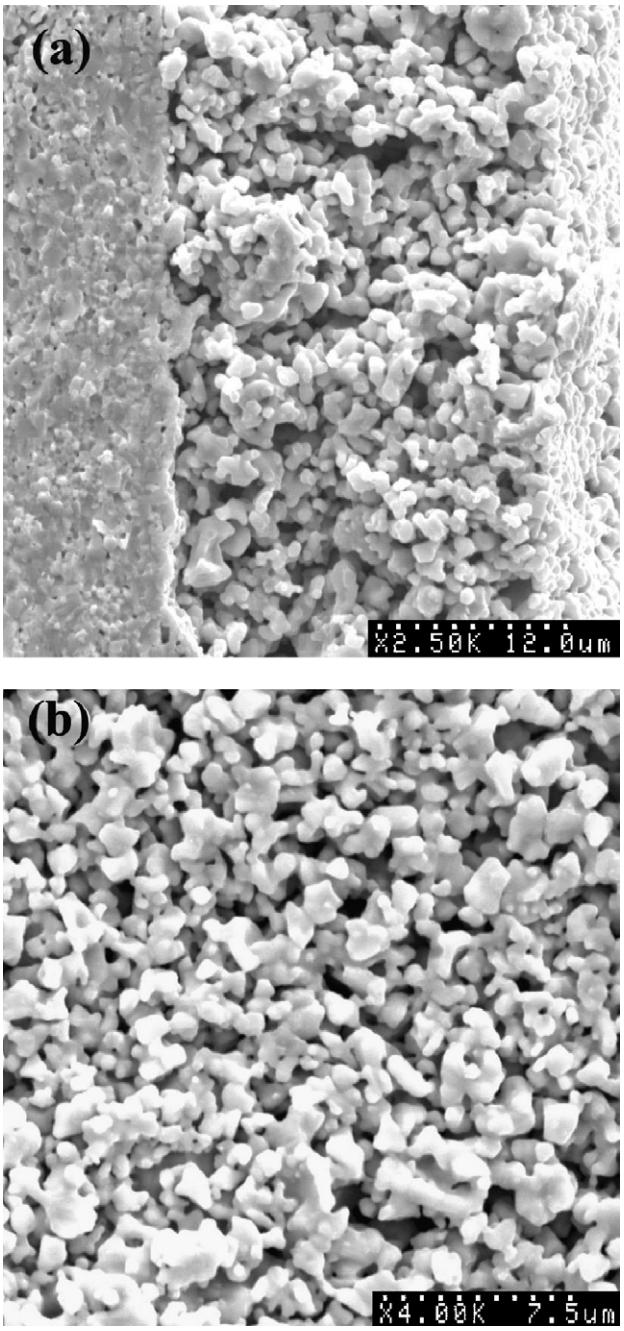

Fig. 9. SEM micrographs of the BSZF cathode: (a) cross-sectional view of SDC–BSZF interface and (b) surface top-view.

cathode to SDC film is also good and the 24 μm-thick electrolyte film is very dense with no cross-membrane cracks. The thickness of BSZF cathodes is about 16–20 μm and the porosity is estimated to be 25–30%, which is suitable for the transport of gases and the electrocatalyst reactions.

3.5. Single cell performance

Fig. 11 shows the temperature dependence of OCVs of the single cell with BSZF cathode operated in air and oxygen. When exposed to air, the OCV of the cell is about 0.8 V at 650 °C. This is lower than theoretical value and the OCV of cells with dense

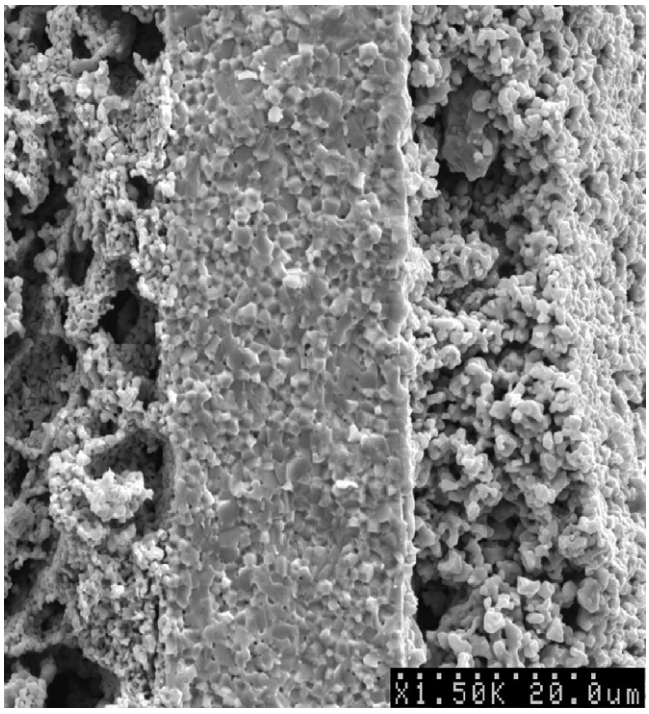

Fig. 10. SEM micrograph of the single cell (cross-sectional view).

YSZ film, which is mainly caused by the reduction of Ce^{4+} to Ce^{3+} at the anode atmosphere [35,36]. The OCV increases with the decreasing of operating temperature, indicating that the reduction of Ce^{4+} is weakened at lower temperatures. When air is switched to oxygen, the cell OCVs increased obviously with an increase of 40–50 mV.

Fig. 12a–c shows the performances of the Ni + SDC anode |SDC film| BSZF cathode single cell. With hydrogen as fuel and stationary air as oxidant, the cell represents the maximum power densities (MPDs) of 392 mW cm^{-2}, 208 mW cm^{-2} and 107 mW cm^{-2} at 650 °C, 600 °C and 550 °C, respectively (Fig. 12a). At 600 °C/0.6 V, the cell exhibits essentially stable performance for 22 h, as shown in Fig. 12b. Higher

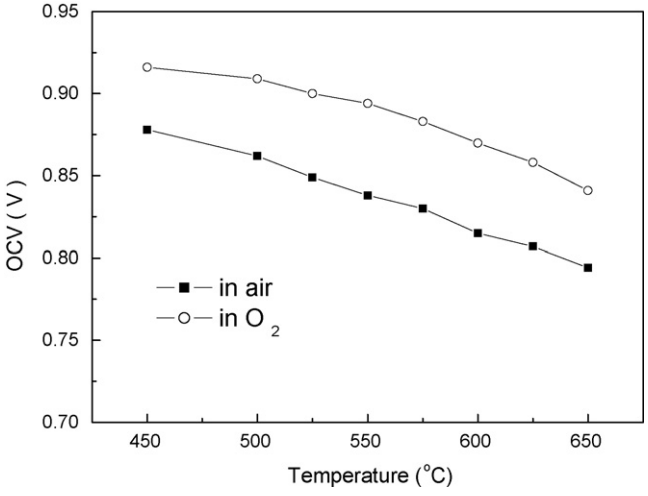

Fig. 11. Temperature dependence of the OCV value for the single cell with BSZF cathode operated in air and oxygen.

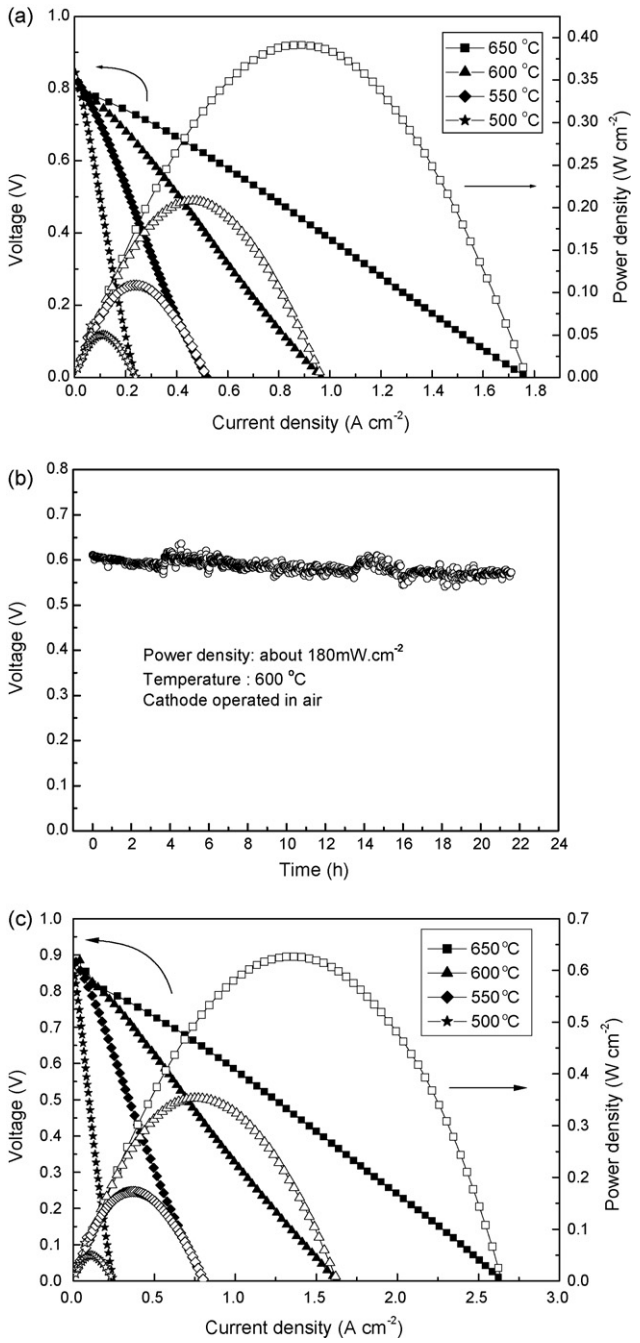

Fig. 12. Performances of the Ni + SDC anode |SDC film| BSZF cathode single cell: (a) *I–V* and *I–P* curves of the single cell with BSZF cathode operated in air, (b) short-term stability of the single cell at 600 °C and (c) *I–V* and *I–P* curves of the single cell with BSZF cathode operated in oxygen flow.

outputs are obtained when the cathode is fed by O_2 flow, maximum power densities of 626 mW cm^{-2}, 353 mW cm^{-2} and 173 mW cm^{-2} are achieved at corresponding temperatures. The obvious improvement of output is mainly ascribed to the enhanced cathode performance; the oxygen reduction process is greatly promoted in higher concentration of oxygen, as can be found in Fig. 5. The polarization resistance of BSZF cathode is reduced from 0.48 Ω cm^2 in simulated air to 0.35 Ω cm^2 in oxygen.

This performance is higher than reported data using other cobalt-free cathodes. With $La_{0.8}Sr_{0.2}FeO_{3-\delta}$ cathode, a cell demonstrated high outputs of 900–950 mW cm^{-2} at 750 °C and 300 mW cm^{-2} at 650 °C with good long-term stability [15]. Using $La_{0.75}Sr_{0.25}CuO_{2.5-\delta}$ as cathode, the YSZ thin film cell showed MPDs of 650 mW cm^{-2} and 280 mW cm^{-2} at 800 °C and 700 °C, respectively [20]. But the performance of our cell is still lower than that with cobalt-based cathode, for example, the cell with SSC–GDC composite cathode exhibited a MPD of 380 mW cm^{-2} at 600 °C [23]. Further optimization of the cathode architecture using advanced methods can result in improvement of cathode/cell performance (e.g. submicro- or nano-sized BSZF particles will increase the electrochemically active sites).

4. Conclusion

In summary, cubic perovskite-type oxide $Ba_{0.5}Sr_{0.5}Zn_{0.2}Fe_{0.8}O_{3-\delta}$ was successfully synthesized and characterized as a novel cobalt-free cathode for the reduced temperature SOFCs. BSZF exhibited a semi-conductive to metal conduction transition at about 590 °C with a maximum conductivity value of 9.4 S cm^{-1}. The polarization resistances of symmetrical BSZF cathode in air were 0.23 Ω cm^2, 0.48 Ω cm^2 and 1.06 Ω cm^2 at 700 °C, 650 °C and 600 °C, respectively. The R_p values were further reduced when operated in oxygen. The approximate $(P_{O_2})^{0.5}$ relationship of R_p with oxygen partial pressure suggested that the oxygen adsorption/desorption process was the reaction rate-limiting step in the measured temperature range. Using BSZF as cathode, a Ni + SDC anode supported, 24 μm SDC thin film cell exhibited maximum power densities of 392 mW cm^{-2} and 626 mW cm^{-2} at 650 °C when stationary air and oxygen flux was used as oxidant, respectively. Further modification of the cathode composition and microstructure will result in improved performance, making BSZF a prospective cathode material for the IT-SOFCs based on doped ceria electrolytes.

Acknowledgements

This research was supported by the Ministry of Science and Technology of China (no. 2007AA05z139 and 2001AA323090). Dr. Gabriel Somesfalean at Harbin Institute of Technology was specially appreciated for the language polishing of the manuscript.

References

[1] J.P.P. Huijsmans, F.P.F. van Berkel, G.M. Christie, J. Power Sources 71 (1998) 107–110.
[2] R. Doshi, V.L. Richards, J.D. Carter, X.P. Wang, M. Krumpelt, J. Electrochem. Soc. 146 (1999) 1273–1278.
[3] B.C.H. Steele, Solid State Ion. 129 (2000) 95–110.
[4] J.B. Goodenough, Ann. Rev. Mater. Res. 33 (2003) 91–128.
[5] N.Q. Minh, J. Am. Ceram. Soc. 76 (1993) 563–588.
[6] I. Yasuda, K. Ogasawara, M. Hishinuma, T. Kawada, M. Dokiya, Solid State Ion. 86 (8) (1996) 1197–1201.

[7] C.R. Xia, W. Rauch, F.L. Chen, M.L. Liu, Solid State Ion. 149 (2002) 11–19.
[8] X.G. Zhang, M. Robertson, S. Yick, C. Deces-Petit, E. Styles, W. Qu, Y.S. Xie, R. Hui, J. Roller, O. Kesler, R. Maric, D. Ghosh, J. Power Sources 160 (2006) 1211–1216.
[9] V. Dusastre, J.A. Kilner, Solid State Ion. 126 (1999) 163–174.
[10] H.J. Hwang, M.B. Ji-Woong, L.A. Seunghun, E.A. Lee, J. Power Sources 145 (2005) 243–248.
[11] E.P. Murray, M.J. Sever, S.A. Barnett, Solid State Ion. 148 (2002) 27–34.
[12] Z.P. Shao, S.M. Haile, Nature 431 (2004) 170–173.
[13] B. Wei, Z. Lu, S.Y. Li, Y.Q. Liu, K.Y. Liu, W.H. Su, Electrochem. Solid State Lett. 8 (2005) A428–A431.
[14] S. Lee, Y. Lim, E.A. Lee, H.J. Hwang, J.W. Moon, J. Power Sources 157 (2006) 848–854.
[15] S.P. Simner, J.F. Bonnett, N.L. Canfield, K.D. Meinhardt, V.L. Sprenkle, J.W. Stevenson, Electrochem. Solid State Lett. 5 (2002) A173–A175.
[16] J.M. Ralph, C. Rossignol, R. Kumar, J. Electrochem. Soc. 150 (2003) A1518–A1522.
[17] K. Huang, H.Y. Lee, J.B. Goodenough, J. Electrochem. Soc. 145 (1998) 3220–3227.
[18] G.Y. Zhu, X.H. Fang, C.R. Xia, X.Q. Liu, Ceram. Int. 31 (2005) 115–119.
[19] S.I. Hashimoto, K. Kammer, P.H. Larsen, F.W. Poulsen, M. Mogensen, Solid State Ion. 176 (2005) 1013–1020.
[20] H.C. Yu, F. Zhao, A.V. Virkar, K.Z. Fung, J. Power Sources 152 (2005) 22–26.
[21] Y.Y. Huang, J.M. Vohs, R.J. Gorte, J. Electrochem. Soc. 151 (2004) A646–A651.
[22] H.H. Wang, C. Tablet, A. Feldhoff, J. Caro, Adv. Mater. 17 (2005) 1785–1788.
[23] C.R. Xia, M.L. Liu, J. Am. Ceram. Soc. 84 (2001) 1903–1905.
[24] B. Wei, Z. Lu, X.Q. Huang, Z.G. Liu, J.P. Miao, N. Li, W.H. Su, J. Am. Ceram. Soc. 90 (2007) 3364–3366.
[25] H. Takahashi, F. Munakata, M. Yamanaka, Phys. Rev. B 57 (1998) 15211–15218.
[26] L.W. Tai, M.M. Nasrallah, H.U. Anderson, D.M. Sparlin, S.R. Sehlin, Solid State Ion. 76 (1995) 259–271.
[27] V.L. Kozhevnikov, I.A. Leonidov, M.V. Patrakeev, E.B. Mitberg, K.R. Poeppelmeier, J. Solid State Chem. 158 (2001) 320–326.
[28] A.L. Shaula, V.V. Kharton, M.V. Patrakeev, J.C. Waerenborgh, D.P. Rojas, F.M.B. Marques, Ionics 10 (2004) 378–384.
[29] B. Wei, Z. Lu, X.Q. Huang, J.P. Miao, X.Q. Sha, X.S. Xin, W.H. Su, J. Eur. Ceram. Soc. 26 (2006) 2827–2832.
[30] S.W. Tao, J.T.S. Irvine, Nat. Mater. 2 (2003) 320–323.
[31] S.Y. Li, Z. Lu, B. Wei, X.Q. Huang, J.P. Miao, G. Cao, R.B. Zhu, W.H. Su, J. Alloy. Compd. 426 (2006) 408–414.
[32] S.Y. Li, Z. Lu, N. Ai, K.F. Chen, W.H. Su, J. Power Sources 165 (2007) 97–101.
[33] Y. Takeda, R. Kanno, M. Noda, Y. Tomida, O. Yamamoto, J. Electrochem. Soc. 134 (1987) 2656–2661.
[34] H. Zhao, L.H. Huo, L.P. Sun, L.J. Yu, S. Gao, J.G. Zhao, Mater. Chem. Phys. 88 (2004) 160–166.
[35] S.P.S. Badwal, F.T. Ciacchi, J. Drennan, Solid State Ion. 121 (1999) 253–262.
[36] M. Mogensen, N.M. Sammes, G.A. Tompsett, Solid State Ion. 129 (2000) 63–94.